Journal of Power Sources 267 (2014) 148–154

Contents lists available at ScienceDirect

Journal of Power Sources

journal homepage: www.elsevier.com/locate/jpowsour

Novel architectured metal-supported solid oxide fuel cells with Mo-doped $SrFeO_{3-\delta}$ electrocatalysts

Yucun Zhou [a], Xie Meng [a], Xuejiao Liu [a], Xin Pan [b], Junliang Li [a], Xiaofeng Ye [a], Huaiwen Nie [a], Changrong Xia [a, b], Shaorong Wang [a, b], Zhongliang Zhan [a, b, *]

[a] CAS Key Laboratory of Materials for Energy Conversion, Shanghai Institute of Ceramics, Chinese Academy of Sciences (SICCAS), 1295 Dingxi Road, Shanghai 200050, PR China
[b] CAS Key Laboratory of Materials for Energy Conversion, Department of Materials Science & Engineering, University of Science & Technology of China, Hefei 230026, PR China

HIGHLIGHTS

- Metal-supported fuel cells are based upon porous 430L |dense YSZ| porous YSZ structures.
- Nominal $SrFe_{0.75}Mo_{0.25}O_{3-\delta}$ oxides are impregnated as symmetrical catalysts.
- Promising power densities of 0.74 W cm^{-2} are obtained at 800 °C.

ARTICLE INFO

Article history:
Received 21 October 2013
Received in revised form
15 February 2014
Accepted 29 April 2014
Available online 21 May 2014

Keywords:
Metal-supported solid oxide fuel cells
Nanostructures
Impregnation
Molybdenum doped strontium ferrite

ABSTRACT

Barriers to technological advancement of metal-supported SOFCs include nickel coarsening in the anode, metallic interdiffusion between the anode and the metal substrate, as well as poor cathode adhesion. Here we report a robust and novel architectured metal-supported SOFC that consists of a thin dense yttria-stabilized zirconia (YSZ) electrolyte layer sandwiched between a porous 430L stainless steel substrate and a porous YSZ thin layer. The key feature is simultaneous use of impregnated nano-scale $SrFe_{0.75}Mo_{0.25}O_{3-\delta}$ coatings on the internal surfaces of the porous 430L and YSZ backbones respectively as the anode and cathode catalyst. Such a fuel cell exhibits power densities of 0.74 W cm^{-2} at 800 °C and 0.40 W cm^{-2} at 700 °C when operating on hydrogen fuels and air oxidants.

1. Introduction

The state-of-the-art SOFCs consist of dense YSZ electrolyte thin films and porous strontium lanthanum manganite (LSM) cathode layers supported in the Ni-YSZ anode cermet substrates [1,2]. Nevertheless, extensive use of expensive and fragile ceramics in the SOFC architecture results in high materials costs and low mechanic reliability. The novel metal-supported solid oxide fuel cell (MS-SOFC), where a porous alloy provides the mechanical support for thin functional anode–electrolyte–cathode layers and simultaneously acts as the anode current collector, emerges as the next generation configuration due to advantages over the traditional all-ceramic counterpart – including excellent structural robustness and stability, high tolerance toward rapid thermal cycling, easy stack assembling as well as low materials cost [3]. In particular, well-established joining techniques such as brazing and welding can be used for the MS-SOFC stack sealing that is able to withstand large thermal gradients and therefore allows for rapid start-up, making the metal-supported SOFC technology competitive in the portable and transportation applications where frequent on-off cycling occurs and quick start-up is expected [4,5].

However, co-firing the Ni-containing anodes with the metallic substrates to densify the electrolyte layers in reducing atmospheres, as required to prevent the metallic supports from oxidation, produced unacceptably large Ni particles due to excessive coarsening that reduced surface area available for fuel oxidation reactions and thereby decreased the fuel cell power densities [6].

* Corresponding author. CAS Key Laboratory of Materials for Energy Conversion, Shanghai Institute of Ceramics, Chinese Academy of Sciences (SICCAS), 1295 Dingxi Road, Shanghai 200050, PR China. Tel./fax: +86 21 6990 6373.
E-mail address: zzhan@mail.sic.ac.cn (Z. Zhan).

http://dx.doi.org/10.1016/j.jpowsour.2014.04.157
0378-7753/

Furthermore, metallic interdiffusion occurred between the Ni-containing anodes and the supporting alloy substrates during high temperature co-firing as well as during the fuel cell operation, reducing the anode catalytic activity and altering the structural property of the metallic substrate as well [7]. Introducing a barrier layer of ceria, gadolinium doped ceria or $La_{0.6}Sr_{0.2}Ca_{0.2}CrO_3$ between the metallic support and the anode could prevent such metallic interdiffusion [7,8]. Alternatively, functional SOFC layers can be fabricated at relatively low temperatures using pulsed laser deposition, reactive sputtering, suspension plasma spraying and atmospheric plasma spraying - this could avoid Ni coarsening, but would lead to high manufacturing costs [9–12]. Impregnating Ni-containing anodes could also avoid Ni coarsening at co-firing temperatures, but the long-term stability of the resulting nano-scale Ni catalysts remains problematic over the long run of fuel cells [13–15].

In addition to Ni coarsening and metallic interdiffusion, application of appropriate cathode layers is another important issue for metal-supported SOFCs. The common cathode catalysts such as LSM would decompose in reducing atmospheres at elevated temperatures if co-fired together with the metal-supported electrolyte structures, and were therefore typically in-situ sintered for MS-SOFCs during the fuel cell operation. Such an approach is problematic in terms of technical reliability and long-term durability due to insufficient interfacial adhesion of the cathode layers on the electrolyte surfaces [6]. Recently, we showed that such a cathode issue could be avoided by impregnating redox-stable Mo-doped $SrFeO_{3-\delta}$ electrocatalysts into the pre-fired porous YSZ backbones [16]. Here we report a novel metal-supported solid oxide fuel cell with impregnated Mo-doped $SrFeO_{3-\delta}$ coatings simultaneously as the anode and the cathode electrocatalysts that display good power densities at reduced temperatures when operating on hydrogen fuels and air oxidants due to their good catalytic activities for hydrogen oxidation and oxygen reduction reactions.

2. Experimental

The new architecture for the metal-supported SOFC was based upon a tri-layer structure—porous 430L | dense YSZ | porous YSZ, which was produced by laminating three tape-cast green tapes with 30 and 50 wt% ammonia oxalate used respectively as the fugitive material for the porous 430L and YSZ layers. The YSZ powders ($7\ m^2\ g^{-1}$) were purchased from Tosoh Corporation (Japan), and the 430L stainless steel powders (−400 mesh) were supplied by Jing-Yuan Powder Material (China). The 430L alloy was chosen as the supporting substrate due to its low costs, compatible coefficients of thermal expansion (CTE) with YSZ electrolytes as well as low oxidation and corrosion rates as desired for extended SOFC longevity [6]. The laminated green tapes were co-fired in a reduced atmosphere of 5% H_2 −95% N_2 at 1320 °C to produce the final structures.

$SrFe_{0.75}Mo_{0.25}O_{3-\delta}$ was selected as the electrocatalysts for both the anode and the cathode due to its good structural stability and mixed ionic-electronic conducting behavior in both oxidizing and reducing atmospheres [17–19] and was added into the porous 430L substrates and the porous YSZ layers using the aqueous solution impregnation method. Throughout the paper, these deposited coatings in a nominal composition of $SrFe_{0.75}Mo_{0.25}O_{3-\delta}$ were denoted as SFMO. Aqueous solutions containing $Sr(NO_3)_2$, $Fe(NO_3)_3 \cdot 9H_2O$, $(NH_4)_6Mo_7O_{24} \cdot 4H_2O$ and citric acid in a molar ratio of 1:0.75:0.0357:2 were impregnated and calcinated at 850 °C in a reduced atmosphere of 5% H_2 − 95% N_2 for 2 h to prevent oxidation of the 430L substrate. These salts were 99% pure and purchased from Sinopharm Chemical Reagent. Each impregnation yielded catalyst loadings (by volume) of 1% in porous 430L and 2% in porous YSZ, and 8–18 impregnation/firing cycles were typically used for the cell fabrication. The quantity of the deposited SFMO catalysts was estimated by the weight difference before and after each impregnation/firing cycle.

For fuel cell tests, silver ink was applied on the electrode surface as the current collector and silver wires were used as the current

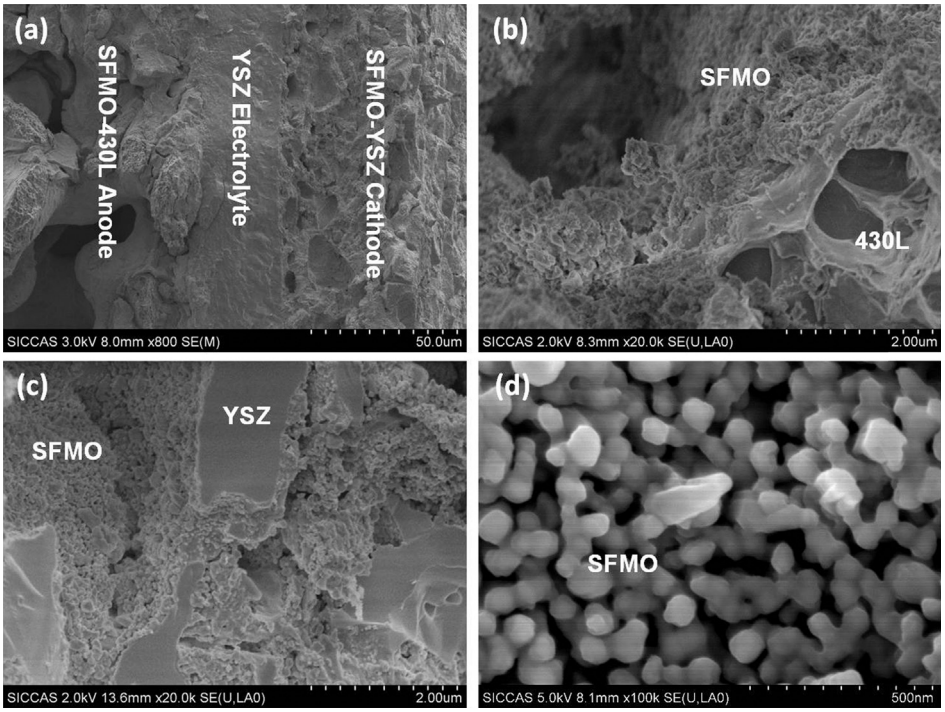

Fig. 1. The SEM micrographs showing the structure of the 430L alloy supported fuel cells. (a) A low magnification survey of the cell. (b) A high magnification view of the SFMO impregnated 430L alloy anode. (c) A high magnification view of the SFMO impregnated YSZ cathode. (d) A high magnification view of the SFMO catalyst.

leads. Current–voltage curves and electrochemical impedance spectra were obtained in a four-probe testing setup over the temperature range of 650–800 °C using an IM6 Electrochemical Workstation (ZAHNER, Germany). The frequency range for impedance measurement was 0.1 Hz–100 kHz. During the measurement, the anode and the cathode were exposed to 97% H_2–3% H_2O and dry air at 100 sccm, respectively. The cell structure was examined using scanning electron microscopy (SEM) in a Hitachi S-4800-II microscope.

The polarization resistances for the SFMO-430L anode and the SFMO-YSZ cathode were determined by testing the SFMO-430L|YSZ|430L-SFMO symmetrical anode cell and the SFMO-YSZ|YSZ|YSZ-SFMO symmetrical cathode cell, respectively. These symmetrical cells were also fabricated using the tape casting, tape lamination and co-sintering techniques. As described above, the SFMO catalysts were added into the porous 430L and YSZ backbones via solution impregnation. The impedance data were collected in the single chamber environment – 97% H_2 – 3% H_2O and dry air at 100 sccm for the symmetrical anode and cathode fuel cell, respectively.

3. Results

Fig. 1(a) shows a representative SEM micrograph of the novel architectured metal-supported SOFCs. The thickness for the porous 430L, dense YSZ and porous YSZ was 300, 18 and 30 μm, respectively. Use of 30 and 50 wt% ammonium oxalate as the fugitive material in the tape formulation yielded a porosity of 40 and 60% for the porous 430L substrate and the porous YSZ layer, respectively. Fig. 1(b) and (c) show SEM micrographs of the SFMO-430L anode at a volume loading of SFMO catalysts V_{SFMO} = 16.0% and the SFMO-YSZ cathode at V_{SFMO} = 32.8% after the fuel cell measurement, respectively. Notably, thin and well intra-connected SFMO layers were coated on the internal surfaces of the porous 430L and YSZ backbones. Fig. 1(d) shows a higher-magnification SEM micrograph of the SFMO coating that exhibited an average particle diameter of ≈60 nm and a pore diameter of ≈40 nm. Such a nano-scale structure has substantially larger surface area than the traditional micron-scale electrode, and therefore allows for fast reaction kinetics on the electrode [20–22]. X-Ray diffraction (XRD) patterns in Fig. 2 confirmed predominant formation of perovskite oxide catalysts in hydrogen in addition to small amounts of metallic Fe precipitates (as discussed later). As observed previously, some minor $SrMoO_4$ impurities were observed for the SFMO catalysts in the cathodes [16].

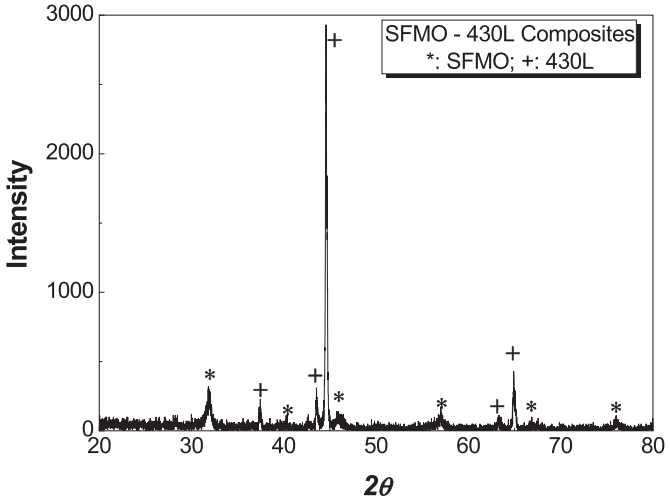

Fig. 2. The X-Ray diffraction patterns of the SFMO-430L composite anodes after the fuel cell measurement.

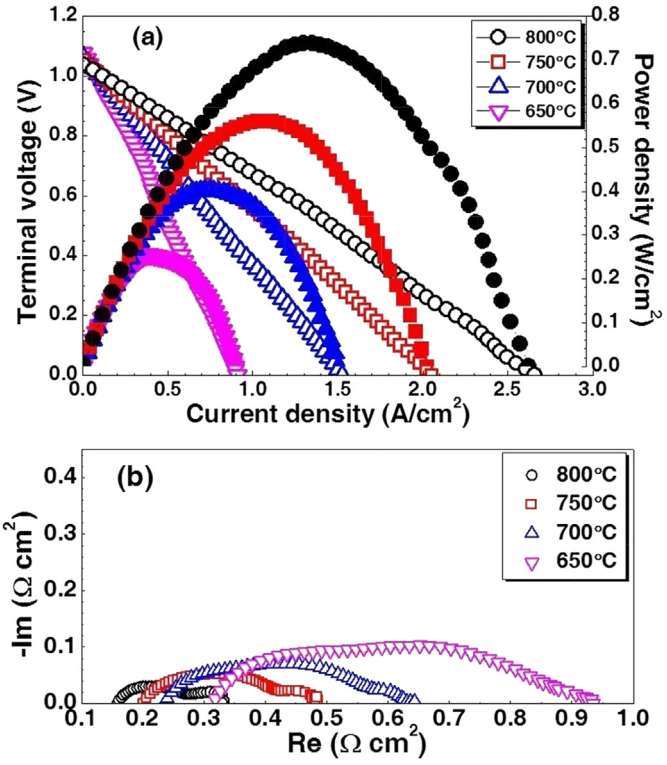

Fig. 3. Characteristics of the 430L alloy supported fuel cell, SFMO-430L | YSZ | YSZ-SFMO, with V_{SFMO} = 16.0% for the anode and V_{SFMO} = 32.8% for the cathode, operating on 97% H_2–3% H_2O fuels and dry air oxidants at 100 sccm over the temperature range of 650–800 °C. (a) Plots of voltage and power density versus current density. (b) The Nyquist plots of impedance spectra at open circuits.

Fig. 3(a) shows cell voltages (V) and power densities (P) as a function of current densities (J) for such a fuel cell, measured at

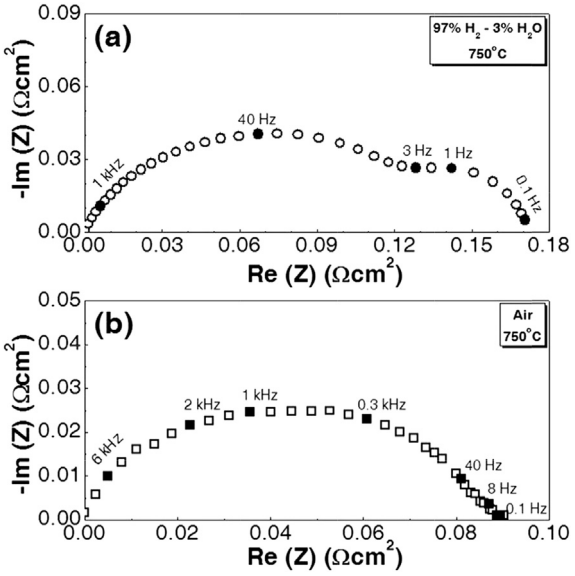

Fig. 4. Polarization analysis on the 430L alloy supported fuel cell. (a) Representative impedance spectra measured at 750 °C for the symmetric SFMO-430L anode fuel cell at V_{SFMO} = 16.0% in humidified hydrogen at 100 sccm. (b) Representative impedance spectra measured at 750 °C for the symmetric SFMO-YSZ cathode fuel cell at V_{SFMO} = 32.8% in dry air at 100 sccm.

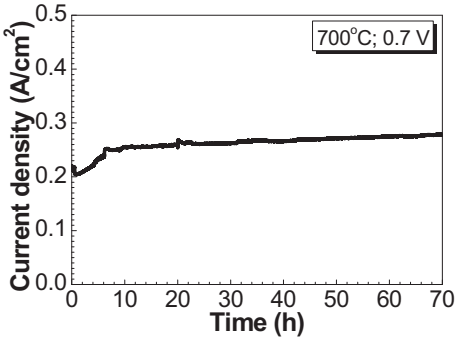

Fig. 5. Stability of the metal-supported SOFC operating on humidified hydrogen fuels and ambient air oxidants at 700 °C and 0.7 V.

temperatures of 650–800 °C with 97% H_2 − 3% H_2O fuels in the anode and dry air oxidants in the cathode both at 100 sccm. The open circuit voltage (OCV) values increased from 1.040 to 1.079 V with decreasing temperature and were within 50 mV of the calculated Nernst potentials, indicative of good gas impermeability of the dense YSZ electrolyte in Fig. 1(a). The maximum power densities measured were 0.74, 0.56, 0.40 and 0.26 W cm^{-2} at 800, 750, 700 and 650 °C, respectively. Fig. 3(b) shows Nyquist plots of the impedance data at open circuits that consist of two or three depressed arcs. The total area specific resistances (R_t) were 0.33, 0.48, 0.64 and 0.94 Ω cm^2, and the overall interfacial polarization resistances ($R_{P,t}$, including both the anode and the cathode) were 0.17, 0.28, 0.41 and 0.62 Ω cm^2 at 800, 750, 700 and 650 °C, respectively.

Impedance measurements were also performed on symmetrical anode fuel cells (SFMO-430L|YSZ|430L-SFMO) and symmetrical cathode fuel cells (SFMO-YSZ|YSZ|YSZ-SFMO) in a uniform atmosphere of 97% H_2 − 3% H_2O for the anode and dry air for the cathode. Representative Nyquist plots of the impedance data at 750 °C are shown in Fig. 4(a) for SFMO-430L anodes and in Fig. 4(b) for SFMO-YSZ cathodes. The pure ohmic resistances due to electrolytes and the conducting wires were subtracted while the interfacial polarization resistances were divided by 2 to account for the contribution of two symmetrical electrodes. Note that these EIS data obtained in single chamber mode should be cautiously

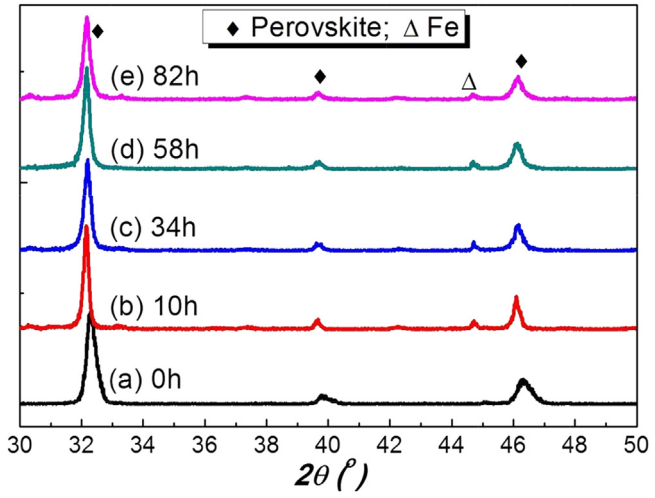

Fig. 6. The XRD patterns of SFMO powders. (a) SFMO as synthesized in air. (b) SFMO reduced at 800 °C in 97% H_2 − 3% H_2O for 10 h (c) SFMO reduced for 34 h (d) SFMO reduced for 58 h (e) SFMO reduced for 82 h.

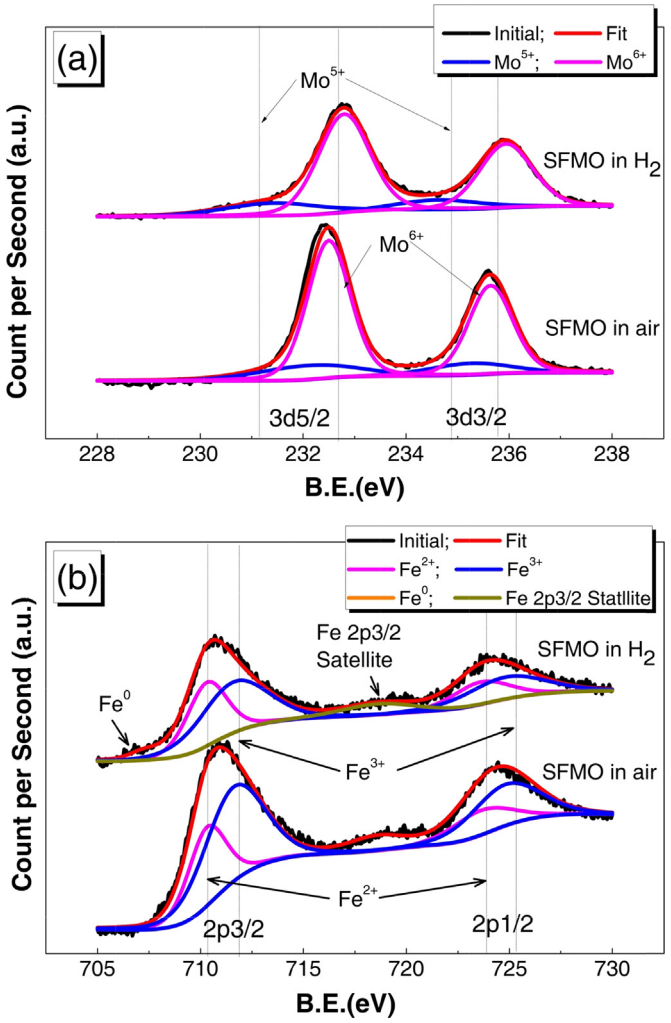

Fig. 7. XPS spectra at room temperature for the SFMO powders as synthesized in air and heat-treated in 97% H_2 − 3% H_2O. (a) Mo 3d XPS spectra. (b) Fe 2p XPS spectra.

correlated with those for functional fuel cells that are exposed to asymmetrical gases, but do provide an effective measure of the catalytic activities of the electrodes for electrochemical reactions. Fig. 4(a) shows that the polarization resistance for the impregnated SFMO-430L anode was $R_{P,A}$ = 0.171 Ω cm^2 at 750 °C, which is impressively low especially given that SFMO catalysts were coated on the internal surfaces of electronic conducting 430L alloys that do not allow for oxide-ionic conduction. Prior reports have shown that the conventionally-sintered and micron-scale SFMO anodes exhibited much larger polarization resistances over much more conducting $La_{0.9}Sr_{0.1}Ga_{0.8}Mg_{0.2}O_{3-\delta}$ (LSGM) electrolytes, *e.g.*, 0.27 Ω cm^2 at 800 °C and 0.45 Ω cm^2 at 750 °C [17], while alternative oxide anodes had to work at much higher temperatures so as to achieve reasonable catalytic activities and produce acceptable $R_{P,A}$ values, *e.g.*, 0.30 Ω cm^2 for $La_{0.75}Sr_{0.25}Cr_{0.5}Al_{0.5}O_{3-\delta}$ on the LSGM electrolytes at 950 °C [23], 0.18 Ω cm^2 for $La_{0.8}Sr_{0.2}Cr_{0.5}Mn_{0.5}O_{3-\delta}$-

Table 1
Atomic percentages of the Mo and Fe elements at different oxidation states.

	Mo^{6+} (%)	Mo^{5+} (%)	Fe^{3+} (%)	Fe^{2+} (%)	Fe (%)
SFMO fired in air	80.4	19.6	65.6	34.4	–
SFMO calcinated in H_2	83.7	16.3	56.2	40.7	3.1

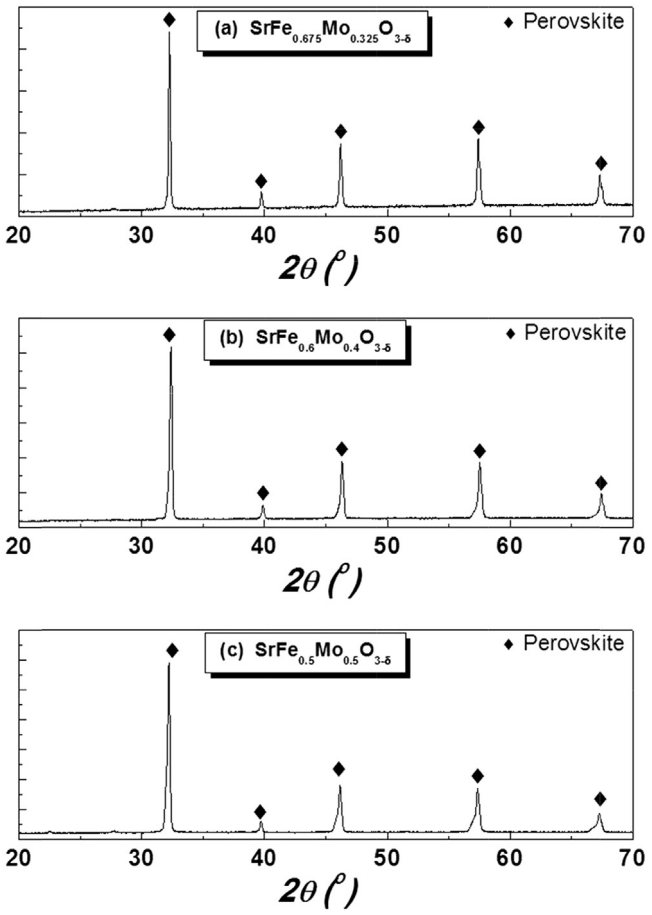

Fig. 8. The XRD patterns of $SrFe_{1-x}Mo_xO_{3-\delta}$ powders as synthesized in 97% H_2 − 3% H_2O. (a) $x = 0.325$. (b) $x = 0.4$. (c) $x = 0.5$.

YSZ on the YSZ electrolytes at 950 °C [24], or 0.35 Ω cm^2 for $La_{0.8}Sr_{0.2}Sc_{0.2}Mn_{0.8}O_{3-\delta}$ on the Sc_2O_3 stabilized ZrO_2 electrolytes at 850 °C [25]. In contrast, the present SFMO impregnated 430L anode exhibited catalytic activities for hydrogen oxidation reactions almost comparable to the conventional micron-scale Ni-YSZ cermets that showed $R_{PA} = 0.1$ Ω cm^2 at 750 °C [26,27]. Fig. 4(b) shows that the polarization resistance was $R_{PC} = 0.090$ Ω cm^2 for the impregnated SFMO-YSZ cathode at 750 °C. Despite the presence of minor $SrMoO_4$ impurities in the deposited SFMO coatings [16], such a low value is still competitive with the conventional micron-scale LSM-YSZ.

Power densities reported here were reasonably good when compared with prior metal-supported fuel cells. For example, a co-fired FeCr alloy supported Ni-YSZ anode and YSZ electrolyte fuel cell with an in-situ sintered $La_{0.6}Sr_{0.4}Co_{0.8}Fe_{0.2}O_3$ (LSCF) cathode showed a relatively low maximum power density of 0.1 W cm^{-2} in hydrogen fuels at 800 °C due to the complicated fabrication issues and the resulting poor catalytic activity of the anode for hydrogen oxidation reactions [6]. Metal-supported fuel cells obtained using the plasma spray technique to deposit the functional SOFC layers as well as the diffusion barrier layer exhibited power densities of 0.4 W cm^{-2} at 800 °C [8]. There are some reports on promising MS-SOFCs with impregnated Ni-containing anodes that yielded initial power densities of ≥0.35 W cm^{-2} at 700 °C [13,14]. Nevertheless, the impregnated Ni-containing anodes showed a pronounced degradation at temperatures even as low as 650 °C due to continuous coarsening of nano-scale Ni catalysts that would reduce the anode catalytic activity and thus increase the anode polarization resistances [14]. In a vivid contrast, the present MS-SOFCs showed

Table 2
Lattice parameters of $SrFe_{1-x}Mo_xO_{3-\delta}$ oxides synthesized in air or hydrogen atmospheres.

Samples	Crystal structure	a(Å)	b (Å)	c(Å)	V(Å^3)
$SrFe_{0.75}Mo_{0.25}O_{-\delta}$ (SFMO) in air	Cubic	7.8438	7.8438	7.8438	482.59
$SrFe_{0.75}Mo_{0.25}O_{3-\delta}$ (SFMO) in H_2	Cubic	7.8816	7.8816	7.8816	489.60
$SrFe_{0.675}Mo_{0.325}O_{3-\delta}$ in H_2	Cubic	7.8772	7.8772	7.8772	488.48
$SrFe_{0.6}Mo_{0.4}O_{3-\delta}$ in H_2	Tetragonal	7.9134	7.9134	7.9443	497.49
$SrFe_{0.5}Mo_{0.5}O_{3-\delta}$ in H_2	Tetragonal	7.9247	7.9247	7.9372	498.46

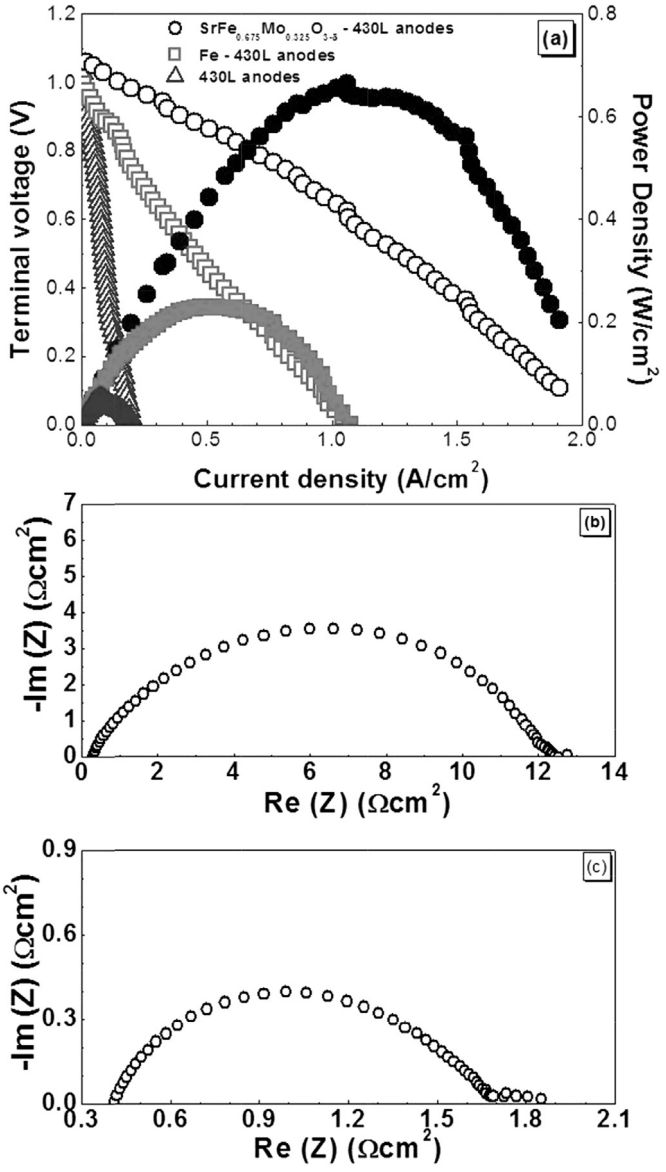

Fig. 9. (a) Plots of voltage and power density versus current density at 800 °C for the 430L alloy supported fuel cells with the $V_{SFMO} = 32.8\%$ SFMO-YSZ composite cathodes. The anodes were the blank 430L supports, the impregnated Fe-430L composites or impregnated $SrFe_{0.675}Mo_{0.325}O_{3-\delta}$-430L composites. Both Fe and $SrFe_{0.675}Mo_{0.325}O_{3-\delta}$ catalysts loadings were 16.0% by volume. (b) Nyquist plots of the impedance data measured at 800 °C for the blank 430L alloy supported fuel cells. (c) Nyquist plots of the impedance data measured at 800 °C for the $V_{Fe} = 16.0\%$ Fe impregnated 430L alloy supported fuel cells.

outstanding stability at 700 °C during the preliminary 70 h durability testing in hydrogen fuels (Fig. 5).

4. Discussion

Electrochemical reactions occurring on the SFMO catalysts consist of several consecutive steps, including gas diffusion within the porous backbones, gas adsorption and desorption on the SFMO catalyst surfaces, surface diffusion and ionization of adsorbed atoms, oxide ion transport in the bulk SFMO coatings and charge transfer at the SFMO|YSZ interfaces [28]. Concerns arise from whether metallic Fe would precipitate out of $SrFe_{0.75}Mo_{0.25}O_{3-\delta}$ oxides in the reducing atmospheres and then promote hydrogen oxidation reactions as the anode catalysts. Given the fact that the presence of 430L made it difficult to identify ferric precipitates based upon the XRD patterns of the anodes in Fig. 2 for the present MS-SOFCs after the fuel cell testing, phase pure SFMO powders were synthesized and heat-treated in 97% H_2– 3% H_2O at different durations. Comparison of XRD patterns shown in Fig. 6 indicates that the reduced SFMO oxide could essentially retain the perovskite structure irrespective of some minor impurities of metallic Fe precipitates. Furthermore, the diffraction peak from ferric at 44.7° in Fig. 6 remained almost constant, indicating that the amount of metallic Fe precipitates did not increase and that the reduced SFMO oxides were stable during the extended exposure in hydrogen atmospheres at 800 °C.

Quantitative analysis of the X-ray photoelectron spectra (XPS) shown in Fig. 7 indicated that 80.4% of the molybdenum element existed as Mo^{6+} for the air-sintered SFMO oxides with the remaining 19.6% as Mo^{5+} while the ferric element consisted of 65.6% of Fe^{3+} and 34.4% of Fe^{2+}, as summarized in Table 1. Upon exposure of the SFMO powders to humidified hydrogen at 800 °C for 10 h, the percentages of Mo^{6+} and Fe^{2+} increased to 83.7 and 40.7 while those of Mo^{5+} and Fe^{3+} decreased to 16.3 and 56.3, respectively. These results indicate that the equilibrium reaction $Fe^{3+} + Mo^{5+} \leftrightarrow Fe^{2+} + Mo^{6+}$ shifts to the right that might be able to explain good stability of SFMO oxides in the reducing atmosphere. Nevertheless, approximately 3% of ferric precipitated out of the oxides and existed in a metallic state, which is in agreement with the small Fe peak observed in the X-Ray diffraction patterns of the SFMO powders after heat-treated in hydrogen (Fig. 6).

In order to determine the chemical composition of the reduced SFMO oxide, additional perovskite oxides including $SrFe_{0.675}Mo_{0.325}O_{3-\delta}$, $SrFe_{0.6}Mo_{0.4}O_{3-\delta}$, $SrFe_{0.5}Mo_{0.5}O_{3-\delta}$ were synthesized by calcinating the corresponding nitrate solutions in air with subsequent heat-treatment in hydrogen at 800 °C for 10 h. XRD patterns of these powders shown in Fig. 8 indicate that all these oxides were phase pure with no metallic Fe precipitates. Structural parameters were obtained by refining these XRD patterns using the MDI Jade 6.0 software and were summarized in Table 2, where the results for the oxidized and reduced $SrFe_{0.75}Mo_{0.25}O_{3-\delta}$ oxides were also included. Tetragonal crystal structures were identified for $SrFe_{0.6}Mo_{0.4}O_{3-\delta}$ with lattice parameters $a = b = 7.9134$ Å, $c = 7.9443$ Å, and for $SrFe_{0.5}Mo_{0.5}O_{3-\delta}$ with $a = b = 7.9247$ Å, $c = 7.9372$ Å. The structures of as-synthesized $SrFe_{0.675}Mo_{0.325}O_{3-\delta}$, oxidized and reduced SFMO were refined as cubic with $a/b/c = 7.8772$, 7.8438 and 7.8816 Å, respectively. Based upon closeness in the crystal structure, it can be concluded that the reduced SFMO oxides consisted predominantly of $SrFe_{0.675}Mo_{0.325}O_{3-\delta}$ other than some minor metallic Fe precipitates.

Prior reports have shown that metallic precipitates were critically important for various oxides to function well as the anodes [29–31]. In order to determine the role of the minor metallic Fe precipitates and the predominant $SrFe_{0.675}Mo_{0.325}O_{3-\delta}$ oxides in the reduced SFMO catalysts for hydrogen oxidation reactions, electrochemical measurements were also performed on three more types of fuel cells: one with the blank 430L anode, another with infiltrated nano-scale Fe and the third with infiltrated nano-scale $SrFe_{0.675}Mo_{0.325}O_{3-\delta}$ with both catalyst loadings at 16.0% by

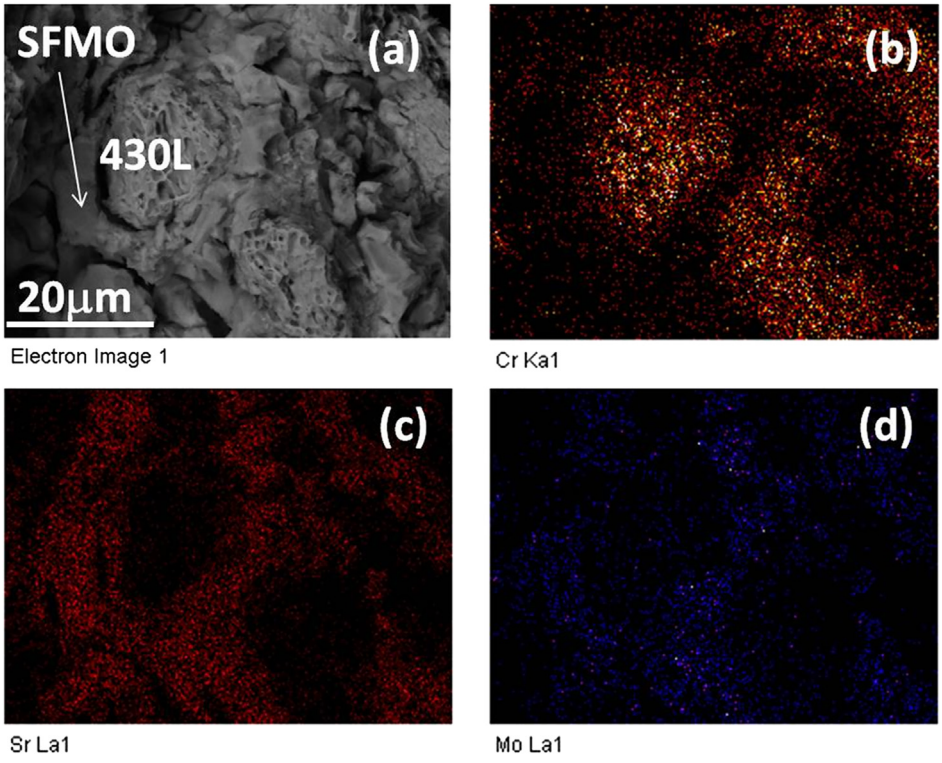

Fig. 10. EDX mapping of the porous SFMO-430L composite anodes for the metal-supported fuel cells operating at 700 °C for 70 h.

volume. Note that the cathodes were the same as described above, *i.e.*, the V_{SFMO} = 32.8% infiltrated SFMO-YSZ composites. As shown in Fig. 9(a), the blank 430L anode fuel cell showed a negligible peak power density of 0.047 W cm^{-2} at 800 °C due to unacceptably large interfacial polarization resistances of ≈12 Ω cm^2 (Fig. 9(b)), implying very poor catalytic activities of the porous 430L supports for hydrogen oxidation reactions. Infiltrating Fe catalysts into the porous 430L backbones increased the fuel cell power density to 0.22 W cm^{-2} with decreased interfacial polarization resistances of ≈1.4 Ω cm^2 (Fig. 9(c)). The most striking observation is that fuel cells with impregnated $SrFe_{0.675}Mo_{0.325}O_{3-\delta}$-430L composite anodes exhibited much higher peak power densities of 0.66 W cm^{-2}, which were almost comparable to the value of 0.74 W cm^{-2} as obtained for MS-SOFCs with impregnated $SrFe_{0.75}Mo_{0.25}O_{3-\delta}$-430L anodes (Fig. 3(a)). Furthermore, the V_{Fe} = 16.0% Fe-430L anode fuel cells were not stable and showed a 40% decrease in the power density even at 650 °C and 0.7 V during a 12-h measurement. Therefore, it could be concluded that it was $SrFe_{0.675}Mo_{0.325}O_{3-\delta}$, the main constituent of the reduced SFMO oxides, that enabled the superior catalytic activities for hydrogen oxidation reactions with negligible contributions from the minor Fe precipitates for the present impregnated SFMO-430L composite anodes.

Note that Cr diffusion is another important issue when the stainless steel is used as the metallic supports. In order to identify whether Cr diffusion occurred during the extended operation, energy-dispersive X-ray spectroscopy (EDX) examination was performed on the metal-supported fuel cells that exhibited good stability at 700 °C for 70 h. The EDX spectrum taken from the porous 430L supports consisted predominantly of peaks corresponding to the Fe and Cr element. On the other hand, only Sr, Fe and Mo peaks were observed in the spectrum taken from the porous SFMO coatings with the Cr peak negligibly small, indicating that Cr diffusion did not occur from the supporting 430L supports to the SFMO catalysts. And very sharp interfaces were observed between 430L supports and SFMO coatings in the overall EDX mappings for the Cr, Sr and Mo elements (Fig. 10). Characterization of the Cr diffusion process was also conducted on a model sample, where the SFMO inks were applied onto the surfaces of porous 430L supports via the screen-printing technique and then heat-treated in humidified hydrogen at 950 °C for 4 h. A relatively higher temperature than typically used for MS-SOFC operation was chosen to accelerate the diffusion kinetics. The individual EDX spectra and the overall EDX mapping for the resulting sample confirmed the absence of Cr diffusion in the present MS-SOFCs.

5. Conclusions

In summary, we have fabricated a novel metal-supported solid oxide fuel cell that features a thin dense YSZ electrolyte layer sandwiched between a porous 430L substrate and a porous YSZ thin layer using economically affordable manufacturing technologies – tape casting, tape lamination and high-temperature co-firing. Simultaneous use of SFMO coatings as the anode and the cathode catalysts, deposited respectively on the internal surfaces of porous 430L and YSZ layers via wet solution impregnation, simplifies the cell fabrication procedure, eliminates Ni coarsening and metallic interdiffusion in the anode, and solves the cathode adhesion issue as well. Based upon symmetrical fuel cell measurements, the area specific polarization resistances at 800 °C were 0.11 Ω cm^2 for SFMO-430L anodes and 0.06 Ω cm^2 for SFMO-YSZ cathodes. The new architectured metal-supported fuel cells exhibited promising power densities of 0.74 W cm^{-2} at 800 °C and 0.40 W cm^{-2} at 700 °C.

Acknowledgment

The authors gratefully acknowledge the financial support of the National Basic Research Program of China (No. 2012CB215401), National Science Foundation of China (No. 51172266), Science and Technology Commission of Zhejiang Province (No. 2011C16037), Chinese Government High Tech Developing Project (No. 2011AA050702), 100 Talents Program of Chinese Academy of Sciences (No. 2009YB001).

References

[1] R.M. Ormerod, Chem. Soc. Rev. 32 (2003) 17–28.
[2] A.J. Jacobson, Chem. Mater. 22 (2010) 660–674.
[3] M.C. Tucker, J. Power Sources 195 (2010) 4570–4582.
[4] M.C. Tucker, C.P. Jacobson, L.C. De Jonghe, S.J. Visco, J. Power Sources 160 (2006) 1049–1057.
[5] Y.B. Matus, L.C. De Jonghe, C.P. Jacobson, S.J. Visco, Solid State Ionics 176 (2005) 443–449.
[6] I. Villarreal, C. Jacobson, A. Leming, Y. Matus, S. Visco, L. De Jonghe, Electrochem. Solid State Lett. 6 (2003) A178–A179.
[7] M. Brandner, M. Bram, J. Froitzheim, H.P. Buchkremer, D. Stover, Solid State Ionics 179 (2008) 1501–1504.
[8] T. Franco, K. Schibinger, Z. Ilhan, G. Schiller, A. Venskutonis, Ecs Trans. 7 (2007) 771–780.
[9] A. Ansar, P. Szabo, J. Arnold, Z. Ilhan, D. Soysal, R. Costa, A. Zagst, M. Gindrat, T. Franco, Solid Oxide Fuel Cells 12 (Sofc Xii) (2011) 147–155, 35.
[10] Y.S. Xie, R. Neagu, C.S. Hsu, X.G. Zhang, C. Deces-Petit, W. Qu, R. Hui, S. Yick, M. Robertson, R. Maric, D. Ghosh, J. Fuel Cell. Sci. Tech. 7 (2010).
[11] N. Oishi, Y. Yoo, J. Electrochem Soc. 157 (2010) B125–B129.
[12] D. Waldbillig, O. Kesler, J. Power Sources 196 (2011) 5423–5431.
[13] M.C. Tucker, G.Y. Lau, C.P. Jacobson, L.C. DeJonghe, S.J. Visco, J. Power Sources 171 (2007) 477–482.
[14] P. Blennow, T. Klemenso, A.H. Persson, K. Brodersen, A.K. Srivastava, B.R. Sudireddy, S. Ramousse, M. Mogensen, Solid Oxide Fuel Cells 12 (Sofc Xii) (2011) 683–692, 35.
[15] Z.B. Liu, B.B. Liu, D. Ding, Z.Y. Jiang, C.R. Xia, Int. J. Hydrogen Energy 37 (2012) 4401–4405.
[16] Y.C. Zhou, X. Meng, X.F. Ye, J.L. Li, S.R. Wang, Z.L. Zhan, J. Power Sources 247 (2014) 556–561.
[17] Q.A. Liu, X.H. Dong, G.L. Xiao, F. Zhao, F.L. Chen, Adv. Mater. 22 (2010) 5478–5482.
[18] A.B. Munoz-Garcia, M. Pavone, E.A. Carter, Chem. Mater. 23 (2011) 4525–4536.
[19] A.B. Munoz-Garcia, D.E. Bugaris, M. Pavone, J.P. Hodges, A. Huq, F.L. Chen, H.C. Zur Loye, E.A. Carter, J. Am. Chem. Soc. 134 (2012) 6826–6833.
[20] D. Han, X.J. Liu, F.R. Zeng, J.Q. Qian, T.Z. Wu, Z.L. Zhan, Sci. Rep Uk 2 (2012).
[21] Z.L. Zhan, D. Han, T.Z. Wu, X.F. Ye, S.R. Wang, T.L. Wen, S. Cho, S.A. Barnett, Rsc Adv. 2 (2012) 4075–4078.
[22] Z.L. Zhan, D.M. Bierschenk, J.S. Cronin, S.A. Barnett, Energy Environ. Sci. 4 (2011) 3951–3954.
[23] J. Pena-Martinez, D. Marrero-Lopez, D. Perez-Coll, J.C. Ruiz-Morales, P. Nunez, Electrochim. Acta 52 (2007) 2950–2958.
[24] J.C. Ruiz-Morales, J. Canales-Vazquez, J. Pena-Martinez, D. Marrero-Lopez, P. Nunez, Electrochim. Acta 52 (2006) 278–284.
[25] Y. Zheng, C. Zhang, R. Ran, R. Cai, Z.P. Shao, D. Farrusseng, Acta Mater. 57 (2009) 1165–1175.
[26] J.S. Cronin, J.R. Wilson, S.A. Barnett, J. Power Sources 196 (2011) 2640–2643.
[27] J.R. Wilson, W. Kobsiriphat, R. Mendoza, H.Y. Chen, J.M. Hiller, D.J. Miller, K. Thornton, P.W. Voorhees, S.B. Adler, S.A. Barnett, Nat. Mater. 5 (2006) 541–544.
[28] X. Meng, X.J. Liu, D. Han, H. Wu, J.L. Li, Z.L. Zhan, J. Power Sources 252 (2014) 58–63.
[29] B.D. Madsen, W. Kobsiriphat, Y. Wang, L.D. Marks, S.A. Barnett, J. Power Sources 166 (2007) 64–67.
[30] C.H. Yang, Z.B. Yang, C. Jin, G.L. Xiao, F.L. Chen, M.F. Han, Adv. Mater. 24 (2012) 1439–1443.
[31] D.M. Bierschenk, E. Potter-Nelson, C. Hoel, Y.G. Liao, L. Marks, K.R. Poeppelmeier, S.A. Barnett, J. Power Sources 196 (2011) 3089–3094.